Multimorphic Materials: Spatially Tailoring Mechanical Properties via Selective Initiation of Interpenetrating Polymer Networks

*Marshall J. Allen, Hsu-Ming Lien, Nathaniel Prine, Carter Burns, Adrian Rylski, Xiaodan Gu, Lewis Cox, Filippo Mangolini, Benny D. Freeman, and Zachariah A. Page**

((This work is dedicated to the memory of Dr. Daniel R King with his inspirational work on hierarchical toughening in soft materials))

M. J. Allen, C. Burns, A. Rylski, Z. A. Page

Department of Chemistry, The University of Texas at Austin; Austin, TX 78712, USA

E-mail: zpage@utexas.edu

M. J. Allen, B. D. Freeman

McKetta Department of Chemical Engineering, The University of Texas at Austin; Austin, TX, 78712, USA

H.-M. Lien, F. Mangolini

Walker Department of Mechanical Engineering, The University of Texas at Austin; Austin, TX, 78712, USA

L. M. Cox

Mechanical and Industrial Engineering Department, Montana State University, Bozeman, Montana 59715, USA

This is the author manuscript accepted for publication and has undergone full peer review but has not been through the copyediting, typesetting, pagination and proofreading process, which may lead to differences between this version and the Version of Record. Please cite this article as doi: 10.1002/adma.202210208.

N. Prine, X. Gu

School of Polymer Science and Engineering, The University of Southern Mississippi, Hattiesburg, MS, 39406 USA

Keywords: interpenetrating networks, photopolymerizations, phase separation, photopatterning, multimorphic

Abstract. Access to multimaterial polymers with spatially localized properties and robust interfaces is anticipated to enable new capabilities in soft robotics, such as smooth actuation for advanced medical and manufacturing technologies. Here, orthogonal initiation is used to create interpenetrating polymer networks (IPNs) with spatial control over morphology and mechanical properties. Base catalyzes the formation of a stiff and strong polyurethane, while blue LEDs initiate the formation of a soft and elastic polyacrylate. IPN morphology is controlled by when the LED is turned 'on', with large phase separation occurring for short time delays (~1-2 minutes) and a mixed morphology for longer time delays (>5 minutes), which was supported by dynamic mechanical analysis, small angle X-ray scattering, and atomic force microscopy. Through tailoring morphology, tensile moduli and fracture toughness can be tuned across ~1-2 orders of magnitude. Moreover, a simple spring model is used to explain the observed mechanical behavior. Photopatterning produces "multimorphic" materials, where morphology is spatially localized with fine precision (<100 μm), while maintaining a uniform chemical composition throughout to mitigate interfacial failure. The fabrication of hinges represents a possible use-case for multimorphic materials in soft robotics.

1. Introduction

Natural materials employ hierarchical structures with 'hard' and 'soft' materials that interact synergistically across molecular to microscopic length-scales to enhance bulk mechanical properties and tailor functionality necessary for survival.[1,2] However, mimicking this hierarchy in synthetic soft materials (e.g., polymers) is an ongoing challenge, and one that promises to facilitate improvements in mechanical tunability, such as tensile strength, toughness, and/or elasticity. To achieve this objective, new chemistries and methods to create such multi-material structures are required.

Synthetic multi-material all-polymeric structures have been previously prepared by spatially tailoring composition, particularly crosslink density.[3–6] For example, Suo and coworkers produced hydrogels comprising a macroscale, densely crosslinked rigid skeleton network (~3 mm minimum dimension) of high modulus in a soft, lightly crosslinked acrylamide matrix, ultimately enhancing

toughness and fatigue resistance (**Figure 1Ai)**.[7] Work by Bowman and coworkers demonstrated synergistic effects in microscale patterned thiol-acrylate materials (~5-100 µm minimum dimension), wherein crosslink density was altered spatially using a photochemical approach.[8] In both systems, a two-stage fabrication strategy was required to introduce the second "material", and the length scale of patterning was found to be a key metric to improve mechanical properties.[8],[9] These materials are reminiscent of double network hydrogels and elastomers, wherein a rigid sacrificial network is embedded in a soft matrix to enhance toughness.[10–12]

This concept of combining two dissimilar polymers to generate a hybrid material with unique and/or improved properties is exemplified by interpenetrating polymer networks (IPNs), in which two networks are interlaced, yet not covalently bound to each other.[13] Mechanical properties in IPNs can be tailored by controlling the morphology, or more specifically, the degree of mixing.[13–20] Early work by Widmaier and coworkers demonstrated that the degree of mixing between two polymer networks could be manipulated kinetically during formation of the two networks. [16],[21–23] Recently the use of orthogonal chemistry in forming IPNs has gone a step further to investigate how differences in initiation and propagation can control morphology, and as a result, mechanical properties. For example, Guymon and coworkers recently showed that light intensity used to induce polymerization could be leveraged as a handle to control the degree of mixing in an acrylate-oxetane monomer system (**Figure 1Aii**).[24] In this example, increasing intensity of UV irradiation (10 to 1500 mW/cm^2) enabled higher degrees of mixing (i.e., smaller domains) and increased strength (2 to 16 MPa) and elongation at break (2 to 8%), corresponding to a 40× increase in strain energy density.[24] In another recent example, Beebe and coworkers demonstrated that semi-IPNs (e.g., one crosslinked and one uncrosslinked network) prepared from sequential polymerization of poly(siloxanes) and poly(methyl methacrylate) were better mixed than the chemically identical IPNs prepared using simultaneous polymerizations, which enabled moduli tunability of 2.5× (i.e., 20 to 50 MPa).[25,26] In these examples, the reliance on a single stimulus for initiation (e.g., light or heat, respectively) precluded the ability to spatially control morphology.

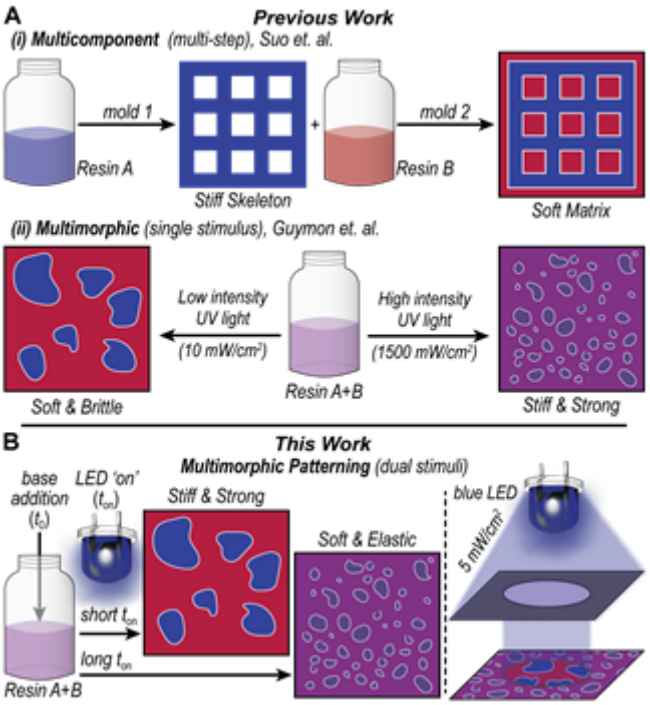

Figure 1. Prior and present work on multimaterial structures. (A) Previous work to improve mechanical performance by (i) Suo et. al.[7] using chemically distinct resins in a two stage process to create mutlimaterial objects and by (ii) Guymon et. al.[24] using light to simultaneously initiate polymerizations for IPN formation and light intensity to tune morphology. (B) This work, where a dual catalyst system is used to tune morphology and mechanical properties spatially, generating multimorphic materials.

Here, orthogonal polymerization mechanisms are leveraged to control IPN morphology with microscopic resolution from a single resin, thus generating "multimorphic" materials. The resultant hierarchical structure was systematically characterized to identify morphology-mechanical property relationships that will inform future designs. Furthermore, bulk mechanical anisotropy was demonstrated by fabricating compositionally uniform all polymeric "hinges".

2. Results and Discussion

The present IPN system comprising polyurethane and polyacrylate networks was prepared in one stage from the corresponding monomeric precursors (**Figure 2A**). A rigid, highly crosslinked polyurethane network was designed using 4,4'-methylenebis(phenyl isocyanate) (MBPI), tetraethylene glycol (TEG), and trimethylolpropane (TMOP), to produce a high glass transition temperature (T_g), rigid plastic. In contrast, 2-(2-ethoxyethoxy)ethyl acrylate, or carbitol acrylate (CA), with 0.3 mol% tetraethylene glycol diacrylate (TEGDA) as a crosslinker was used to form a soft, low T_g acrylate network. Furthermore, the similar functionality (and polarity) between the TEG and CA facilitated mixing of the two monomeric precursors, along with swellability of the fully formed

polyurethane network by the acrylate solution (Figure S1). A mass ratio of 61:39 acrylate to combined urethane monomers was used for all materials in this work (Table S1). Other monomers attempted include aliphatic isocyanates that had lower reactivity compared to corresponding aromatic isocyanates, phenols that inhibited radical formation, and various acrylates that resulted in a smaller difference in mechanical properties relative to CA (Figure S2-S4 and Table S2-S3).

Orthogonal control over each polymerization was achieved using a dual initiation strategy. The polyurethane network was initiated through the physical introduction of base, 1,4-diazabicyclo[2.2.2]octane (DABCO), which catalyzed reaction between isocyanate- and alcohol-containing monomers/crosslinkers. The acrylate polymerization was initiated indirectly via irradiation from a blue LED panel (460 nm center wavelength, ~5 mW/cm^2 intensity, Figure S5), which activated a two-component photoredox system, namely camphorquinone (CQ) and ethyl-4-dimethylamino benzoate (EDMAB). In this manner, a resin containing monomers and the photosystem could be initiated by either or both mechanisms (base or light) to produce a single network or mixed IPN.

To assess polymerization orthogonality, real time attenuated total reflectance Fourier Transform infrared (ATR-FTIR) spectroscopy was employed, monitoring the disappearance of isocyanate (2200 cm^{-1})[27] and alkene (900 cm^{-1})[27] signals as a function of time (**Figure 2B**). Upon addition of DABCO, in the absence light, isocyanate functionality was fully consumed in ~14 minutes, while little-to-no acrylate conversion was observed (**Figure 2B**, left). In contrast, turning the light 'on' ~60 seconds after adding DABCO resulted in simultaneous monomer (isocyanate and alkene) consumption that completed within ~14 minutes (**Figure 2B**, middle). In the absence of DABCO, irradiation resulted in acrylate conversion at a comparable rate to when the base was incorporated (**Figure 2B**, right). Although, isocyanate conversion occured in the absence of DABCO, it arose from uncatalyzed urethane formation as opposed to cross-reactivity with the acrylate, which was supported by a control experiment where neither base addition nor light irradiation was done, showing a comparable rate of background isocyanate conversion (Figure S6).

Important to the reaction dynamics are the distinct mechanisms by which each polymerization proceeds. Polyurethane formation occurs via step-growth and polyacrylate by chain-growth. As such, in the absence of base, ~40% isocyanate conversion occurs at the time of full acrylate conversion, which corresponds to predominantly dimer formation (**Figure 2B**, dashed line at 50% conversion). Moreover, gelation was estimated to occur at 93% conversion for the urethane, based on Carothers equation[28] for step-growth polymerizations—significantly higher than that of the chain-growth

acrylate. This was further supported by (photo)rheology, which provided times to gelation of 5.7 ± 0.7 minutes and 2.3 ± 0.3 minutes for the urethane and acrylate systems, respectively (Figures S10). In combination with real time ATR-FTIR spectroscopy, these gel points determined via (photo)rheology corresponded to conversions of 91 and 11% for urethane and acrylate, respectively (**Figure 2B** red and blue lines, respectively).

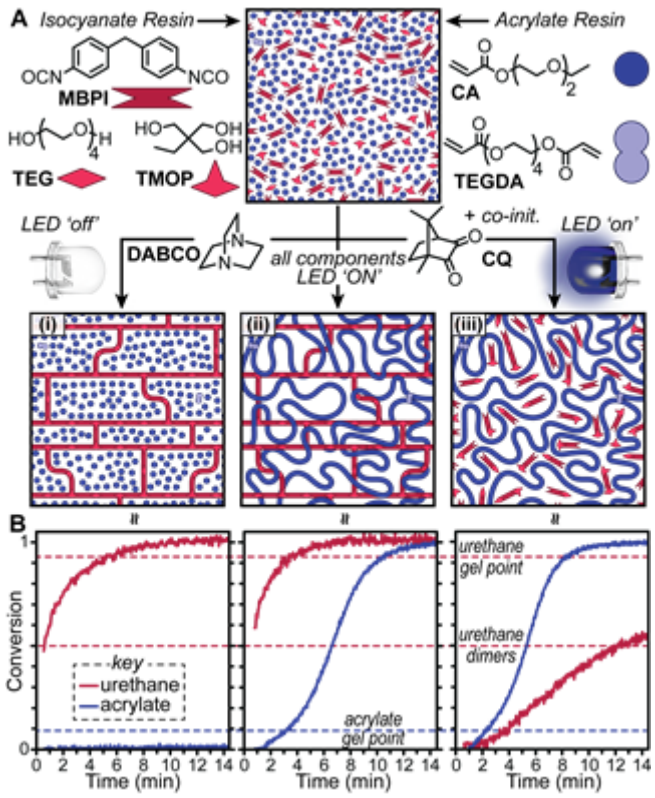

Figure 2. Overview of materials, conditions, and polymerization kinetics for polyurethane and polyacrylate formation. (A) Chemical composition and corresponding symbols representing urethane (left) and acrylate (right) resin components, along with schematics of networks formed under base addition and/or light irradiation. (B) Isocyanate and acrylate conversion as a function of time under three different conditions, characterized with ATR-FTIR spectroscopy. The three conditions were base addition in the absence of light (left), base addition with light 'on' (middle), and light 'on' without base. Time = 0 corresponds with DABCO addition. MBPI, 4,4'-methylenebis(phenyl isocyanate); TEG, tetraethylene glycol; TMOP, trimethylolpropane; CA, carbitol acrylate; TEGDA, tetraethylene glycol diacrylate; CQ, camphorquinone; EDMAB, ethyl-4-dimethylamino benzoate.

The effect of light 'on' time (t_{on}) for IPN formation was characterized to identify the scope and morphological tunability of the present system. Thin film samples (~250 µm) were prepared by casting the mixture between glass plates and varying t_{on} between 1 and 30 minutes, where addition of DABCO corresponds to t_0 (**Figure 3A**). Post-irradiation, all films were soaked in a 1:1 isopropanol-water mixture to remove catalyst, solvent, and terminate any unreacted isocyanate, followed by drying under vacuum at 80 °C for ~15 hours. It was immediately evident that t_{on} influenced

morphology by the difference in visible transparency, with short t_{on} values providing fully opaque films and long t_{on} values resulting in transparent ones (Figure S11). Samples were then punched from the thin films and subjected to dynamic mechanical analysis (DMA). At short t_{on} (~1-2 min., opaque samples), distinct tan δ transitions, representative of glass transition temperatures (T_g), were present at ~52 and 100 °C (**Figure 3B**). These values correlate with those observed for the pure polyacrylate and polyurethane networks, respectively (Figures S12-S13). Thus at short t_{on}, pure regions of the two polymers exist (i.e., phase separation occurs during IPN formation). However, at longer t_{on}, the tan δ peaks begin to merge, creating a broader transition indicative of a more mixed morphology.[13] Regardless of t_{on}, key FTIR peaks of the pure networks were detected in equal proportions in the final IPN films (Figure S14-S15).

To explain this observation, we proposed that polyacrylate formation induces phase separation when it occurs prior to polyurethane gelation, as shown schematically in **Figure 3C** for short and long t_{on}. This hypothetical phase-separated morphology for short t_{on} is supported by the distinct step- and chain-growth mechanisms, where small molecule urethanes (e.g., dimers and oligomers) would be present at high isocyanate conversion and able to diffuse away from the high molecular weight polyacrylate chains formed at low acrylate conversion. In contrast, for long t_{on}, formation of continuous polyurethane domains prior to polyacrylate formation would mitigate phase separation, and result in smaller, more mixed domains. Atomic force microscopy coupled with infrared spectroscopy (AFM-IR) was used to confirm the proposed morphologies for short (t_{on} = 1 min.) and intermediate (t_{on} = 6 min.) time delays, while longer time-delays proved too difficult to analyze due to an instrument resolution limit of ~10 nm (**Figure 3D**). Monitoring the AFM-IR response upon excitation at 1603 cm^{-1} and 1731 cm^{-1} that were specific to urethane and acrylate (ester) functionalities, respectively, revealed large, well defined globules of acrylate (~180 ± 40 nm) in a matrix of urethane for t_{on} = 1 min., while t_{on} = 6 min. resulted in smaller and less defined domains, indicative of mixing. This was further supported by small angle X-ray scattering (SAXS) that showed a similar decrease in phase separation between the two domains as t_{on} was increased, evidenced by a shift in the scattering peaks to higher scattering vector values (Figure S16). Notably, the scattering peaks are diffuse (i.e., broad), suggesting a broad distribution of domain sizes commonly observed for binary phase-separated systems. Despite the dramatic differences in morphology, the resultant films are chemically identical, as evidenced by gravimetric analysis showing consistent mass loss for processed samples (Figure S18), along with ATR-FTIR of the processed films (Figure 3E, Figure S15).

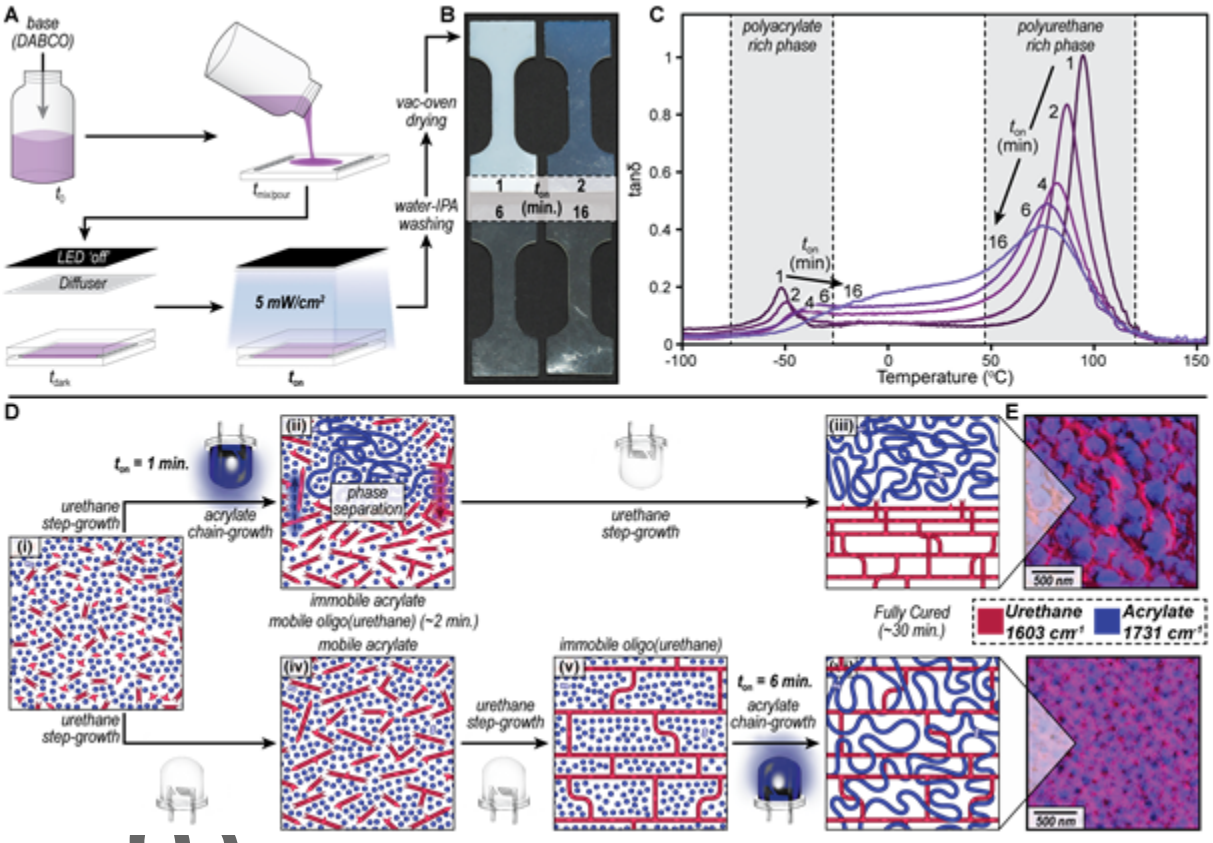

Figure 3. Preparation and morphological characterization of polyurethane/polyacrylate IPNs. (A) Schematic illustration of the film casting process, where t_0 represents DABCO addition and t_{on} the time at which irradiation begins. (B) Digital images of samples prepared with t_{on} of 1, 2, 6, and 16-min., showing disparate opacity. (C) Dynamic mechanical analysis (DMA) of films pictured in A, cast with a DABCO concentration of 100 mM. (D) Proposed mechanism for morphologies formed with short (top) and long (bottom) t_{on}. (E) AFM-IR overlays of urethane and acrylate (ester) absorption signals for films prepared with t_{on} = 1 min. (top) and t_{on} = 6 min. (bottom).

To identify the effect of morphology on mechanical properties, IPNs, pure polyurethane and polyacrylate samples were subjected to uniaxial tension, monitoring the stress-strain response (**Figure 4A**). The pure polyurethane was a stiff, strong, and brittle plastic, while the pure polyacrylate was soft and elastic (Table S11). The IPNs on the other hand had hybrid properties that were strongly dependent on t_{on}. Short t_{on} (~1 min.) values resulted in stiff and strong plastics that yield and neck, with a Young's moduli (E) of 400 ± 30 MPa and yield stress (σ_y) of 12 ± 0.4 MPa. In contrast, long t_{on} (~30 min.) resulted in a soft and elastic material, with E = 5 ± 2 MPa and little hysteresis upon cycling to 75% strain (Figure S20 and Movie S1-S2). IPNs prepared with intermediate t_{on} consistently provided materials with intermediate properties between short and long t_{on}. Thus, the present system enables mechanical properties to be precisely tuned by simple toggling of a light switch (i.e., turning 'on' an LED) at different times post-base (DABCO) addition.

The concentration of base (DABCO) in the mixture was a subsequent handle that was assessed to determine its effect on morphology and mechanical properties (**Figure 4B**). Decreasing the DABCO concentration from 100 to 75 and 50 mM resulted in slower polyurethane network formation, as indicated by ATR-FTIR and (photo)rheology results (Figure S7 and Figure S10). However, the mechanical properties of the resulting IPNs showed the same transition from a stiff/strong plastic to a soft/elastic material as t_{on} increased, albeit with different kinetics, along with having similar upper and lower moduli bounds that were different by ~2 orders of magnitude (~400 to 5 MPa). Notably, the transition away from a stiff plastic (i.e., a drop in modulus) occurred when t_{on} was past the polyurethane gel points, which were 2.9 ± 0.2, 4.1 ± 0.3, and 5.5 ± 0.6 for 100, 75, and 50 mM, respectively. Furthermore, plotting isocyanate conversation at t_{on} *vs* E collapses all DABCO concentrations onto a single line (Figure S24**)**, indicating that the extent of network formation at t_{on} is a key parameter that governs final IPN mechanical properties. Therefore, DABCO concentration provides a tunable handle to predictably tailor polymerization/phase-separation kinetics, and in-turn facilitate different processing windows to access IPNs with disparate mechanical properties.

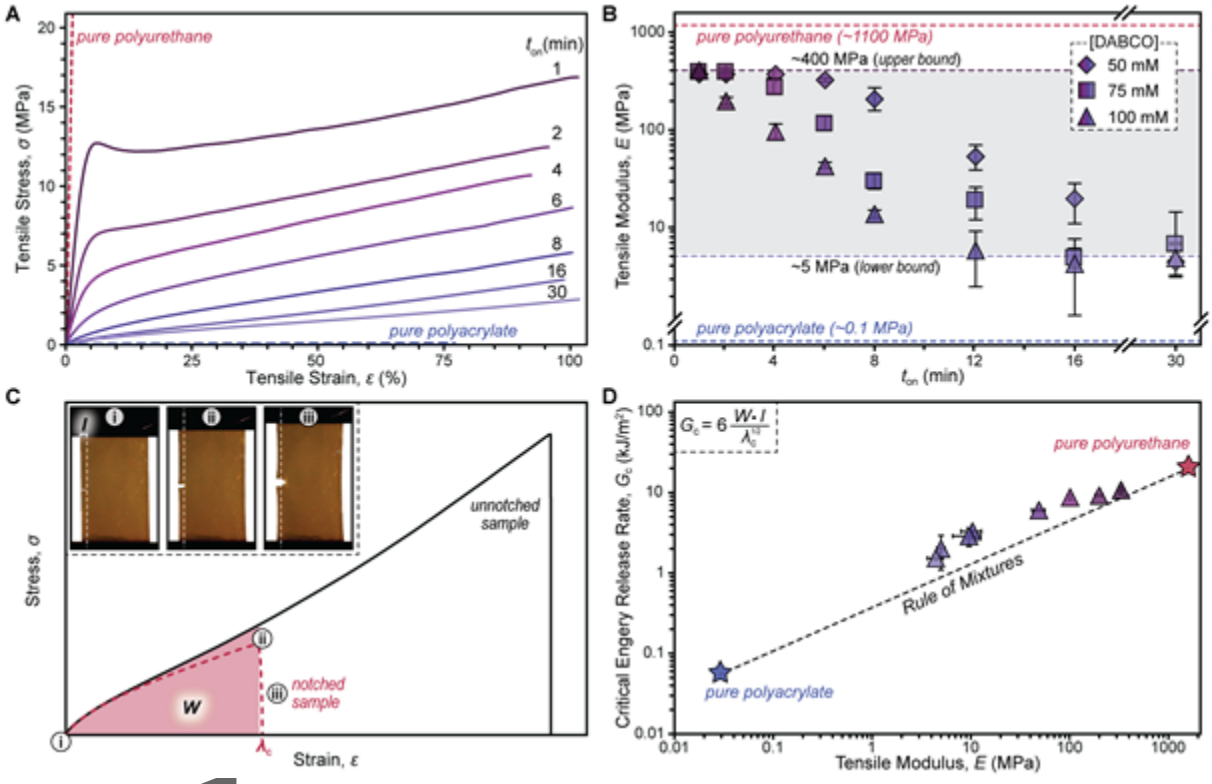

Figure 4. Mechanical characterization of IPNs under uniaxial tension relative to pure polyurethane and polyacrylate materials. (A) Representative stress-strain data for IPNs prepared using variable t_{on}. (B) Average tensile modulus as a function of t_{on} with variable base (DABCO) concentration for IPN preparation. Each data point represents the average of at least 3 samples with error bars being ±1 standard deviation from the mean. (C) Representative notch test for IPN prepared with a t_{on} = 12 min., which was used to calculate critical energy

release rate (G_c), an estimate of fracture toughness. Inset – images of sample during a notch test with corresponding positions on graph represented as (i), (ii), and (iii). (D) G_c relative to tensile modulus, showing that IPNs follow the "rule of mixtures", as represented by the dashed line. Equation for G_c calculation provided as an inset. Each data point represents the average of 3 samples with error bars being ±1 standard deviation from the mean.

To estimate fracture toughness, critical energy release rate (G_c) was measured (**Figure 4C**), which is a material property that dictates when defects will begin to propagate as cracks, leading to failure in materials/objects. Analogous to E, G_c increased with decreasing t_{on}, having a maximum value of 11 ± 1 kJ/m^2 (t_{on} = 1 min.) and a minimum of 1.5 ± 0.1 kJ/m^2 (t_{on} = 30 min.). For context, natural rubber had a G_c value of ~10 kJ/m^2 (Figure S28), indicating that the present IPNs are relatively tough materials. The G_c values for IPNs prepared with intermediate t_{on} values fell between these two, and additionally followed the "rule of mixtures"[[8]] when comparing to G_c values of pure polyurethane (0.05 ± 0.02 kJ/m^2) and pure polyacrylate (20 ± 2 kJ/m^2) (**Figure 4C**). This trend indicates that morphology predictably governs fracture energy, which enables fine tuning of mechanical properties without needing to change material composition.

To better understand how the observed change in morphology affected modulus, AFM measurements were performed on the surface of cross-sectioned films both in fast force mapping (FFM) mode fit to a Hertzian contact model (**Figure 5A**) and amplitude-modulation/frequency modulation (AM-FM) mode (Figure S31), providing similar results. For short t_{on} values, a continuous rigid polyurethane matrix with a maximum contact modulus on the order of ~1 GPa was observed around soft polyacrylate globules with a minimum contact modulus of ~1 MPa, along with an intermixed region of functionally graded modulus between the domains (**Figure 5A**). The average modulus within the globules was measured to be ~25 MPa, which is higher than that of pure polyacrylate. This is hypothesized to arise from the need to apply a force of 20 nN for accurate measurements, which corresponds with an indentation depth of 82 ± 6 nm. Given an indentation depth on the same order of magnitude as the globule domain sizes, the AFM probe is expected to partially actuate the stiffer surrounding matrix. For long t_{on} values, no continuous matrix was observed. Rather, co-continuity between intermixed and soft regions, consistent with AFM-IR results (**Figure 3D**). The reduction in domain size with longer t_{on}, was consistent with SAXS measurements and correlated well with the reduction in bulk modulus (**Figure 5B**).

To draw a relationship between morphology and modulus, a three component Takayanagi model[29] was employed wherein the material was treated as intermixed-encased acrylate globules embedded in a rigid polyurethane matrix (**Figure 5C**, Equation S4). Discussion on selection of this model can be found in the supporting information (note that apparent modulus is used in place of

complex modulus to describe the present quasi-static measurements). The combined AFM and SAXS results imply smaller domain spacings lead to a decrease in the volume fraction of pure urethane and an increase in volume fraction of intermixed regions, thereby reducing modulus. By assuming a constant chemical composition for the bulk film and individual domains, a theoretical relationship between the volume fraction of matrix and E_{bulk} was generated (**Figure 5D**). Volume fractions of intermixed region, estimated from AFM data (Table S17), agreed well with those predicted from the Takayanagi model to produce the bulk moduli observed in mechanical testing (**Figure 5D**). When the estimated volume fractions were applied to the model, predicted E_{bulk} values of 540 and 2 MPa, for a t_{on} values of 1 and 30 minutes, respectively. This result is in good agreement with the E values of ~400 MPa and 5 MPa from tensile testing (**Figure 4B**).

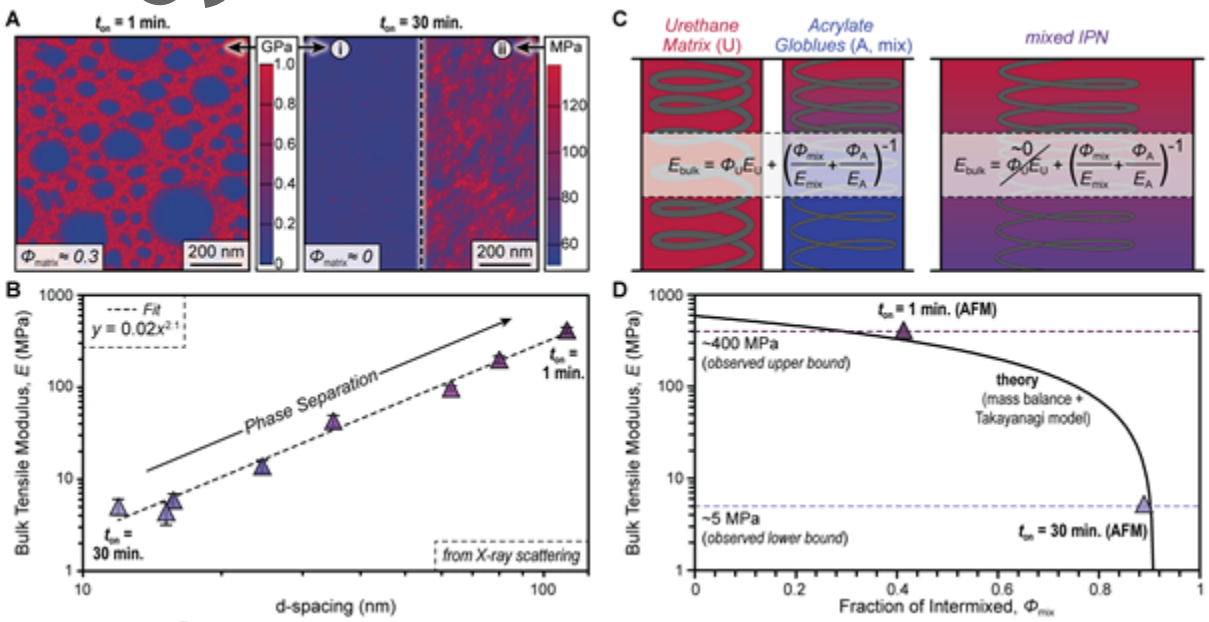

Figure 5. Predicting bulk tensile modulus (E_{bulk}) of IPNs by correlating morphology from AFM nanomechanical mapping to forces experienced during uniaxial strain. (A) AFM mechanical mapping for t_{on} = 1 min. (left) and t_{on} = 30 min. (right), with the latter being plotted on the same modulus scale (i) as the former and separate, narrower modulus scale (ii) for clarity. (B) Domain spacing, estimated as $2\pi/q^*$ obtained from SAXS plotted against the sample's bulk tensile modulus. (C) Three-component Takayanagi model for fully phase-separated (left) and mixed (right) IPNs as the fraction of urethane matrix approaches zero. Φmix was measured from the images, as described in the SI. (D) Plot of bulk tensile modulus versus fraction of intermixed phase. The black line represents the predicted trend using a mass balance combined with the Takayanagi model shown in C. Triangles represent the observed tensile modulus and estimated volume fraction of the intermixed region from AFM. Dotted lines are the observed bulk moduli for the hardest and softest IPNs observed.

Multimorphic hierarchical materials were targeted by leveraging the effect of t_{on} on morphology and mechanical properties with that of the spatial control offered by light-induced polymerizations (**Figure 6**). Using a photomask, two t_{on}'s could be accessed locally by first irradiating regions shortly after mixing (t_{on} = 1.5 min.) followed by removal of the photomask and subsequent irradiation (t_{on} ≥

16 min.) of the entire film (**Figure 6A,** Figure S32). In-turn, a single resin was used to prepare patterned films with well-defined stiff/strong and soft/elastic regions. The distinct transmittance of the two regions (opaque = stiff and transparent = soft) enabled visual characterization of resolution. As such, films prepared with a USAF 1951 photomask having a thicknesses of ~250 um were characterized using backlit digital microscopy, which revealed a resolution of ~128 lp/mm (i.e., ~4 μm features) (**Figure 6B,** Movies S3-S4).

Mechanical characterization of films with lines of varying widths (5 mm to 50 μm) was employed to examine "mechanical resolution". This was motivated by prior observation of that transparent films that were visually indistinguishable, yet mechanically disparate (*E* from ~150-5 MPa). Uniaxial tension of samples with patterned lines perpendicular and parallel to the direction of strain provided moduli that were in good agreement with the models for large, 5 mm features; 123 ± 16 MPa and 22 ± 10 MPa, for parallel and series, respectively (**Figure 6C**). However, experiment deviated from theory for smaller lines, with no significant difference in moduli for lines <250 μm.

Nanoindentation across interfaces of the line-patterned samples was used to further characterize mechanical resolution. Indentations were performed every 50 μm, providing a clear difference in contact moduli for the 5 mm features in going from long to short t_{on}, namely 25 ± Y MPa to 300 ± Y MPa, respectively (**Figure 6D**). Moreover, the difference in contact moduli had a gradient transition region of ~250 μm, which is in good agreement with the mechanical resolution observed for the tension experiments. For line spacings <250 μm, little difference in contact moduli was observed. The loss in mechanical resolution for photopatterned samples was hypothesized to arise from overcure that could be exacerbated by the use of an inexpensive non-collimated LED panel, internal scattering upon phase-separation, internal reflection, and/or monomer gradients that arise during polymerization to drive diffusion across interfaces. The latter hypothesis was supported by experiments with varying DABCO concentrations, showing improved pattern resolution when using higher concentrations, where diffusion would be limited by faster polymerizations (Figure S35). It is thus anticipated that higher pattern fidelity could be achieved by increasing polymerization rates and improving the optical setup (e.g., collimated light source and refractive index matched interfaces).

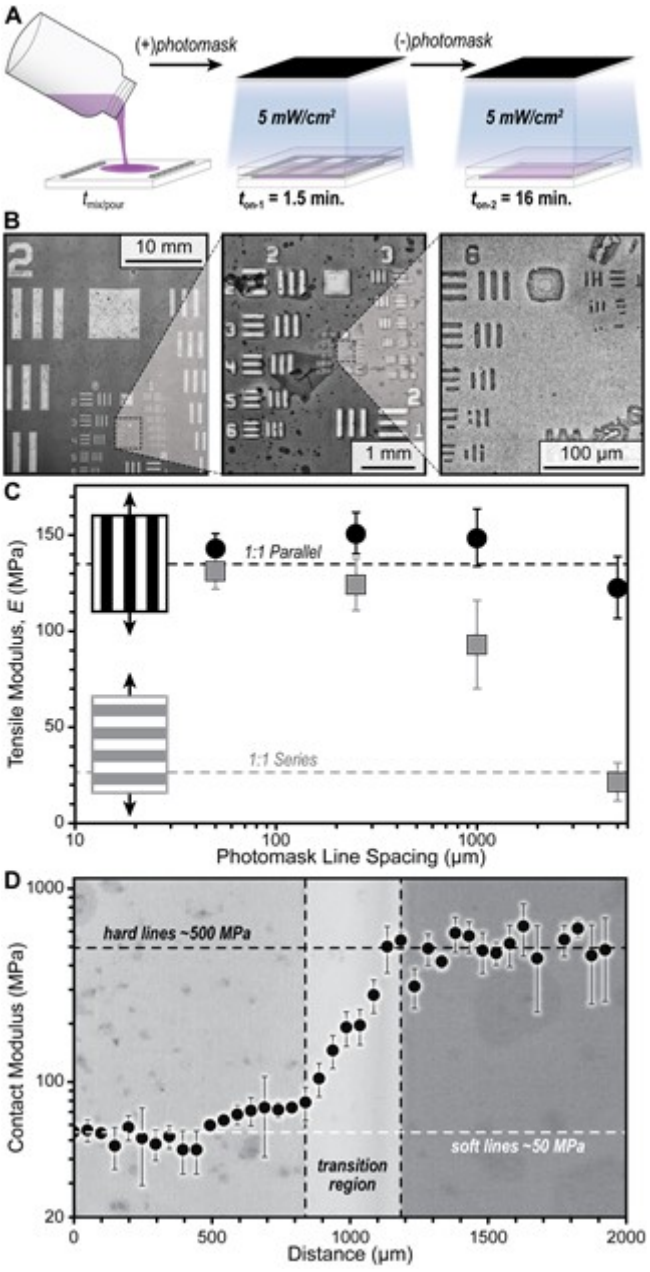

Figure 6. Characterizing optical and mechanical resolution of photopatterned multimorphic samples. (A) Schematic representation of the photopatterning process. (B) Digital (microscopy) images of a USAF 1951 resolution pattern, showing an optical resolution of ~4 µm. (C) Average tensile moduli of line-patterned films tested with hard-soft regions in parallel (black circles) and series (grey squares). Each data point represents the average of 3 samples with error bars being ±1 standard deviation from the mean. (D) Contact moduli from nanoindentation across a soft-to-hard interface on a 5 mm line-pattern sample, where each point represents the average of 6 indentations performed at the same longitudes across a single sample. Data overlayed on the corresponding optical image. Error bars represent ±1 standard deviation from the mean.

As a representative application of multimorphic materials, soft hinges were fabricated and characterized with bending tests. Films with alternating hard-soft-hard lines were prepared and subjected to a full 180° bend by hand, both perpendicular and parallel relative to the soft (long t_{on})

line. The hinge bent perpendicular to the soft hinge resulted in creasing, a permanent deformation (**Figure 7Aii** and Movie S5), matching the behavior observed for the pure hard control sample (**Figure 7Ai**). In contrast, the sample was able to rebound after bending parallel to the soft line, returning to the original shape without an observable crease (**Figure 7Aiii**), matching the behavior of the pure soft control sample (**Figure 7Aiv**). This qualitative bending experiment was performed in an analogous fashion using a three-point bending test on DMA to quantify the associated stress; (i.e., ease of bending along the different hinge axes). Bending perpendicular to the soft line showed a similarly high bending stress relative to the stiff, short t_{on} control material, while bending parallel to the soft line had a similarly low stress relative to the soft, long t_{on} control material. Overall, a 20× difference in bending stress was measured for the hinge when deforming perpendicular vs. parallel to the soft line. Therefore, multimorphic materials hold promise for utility in applications that would benefit from anisotropic bending stress, such as joints in soft robotics.

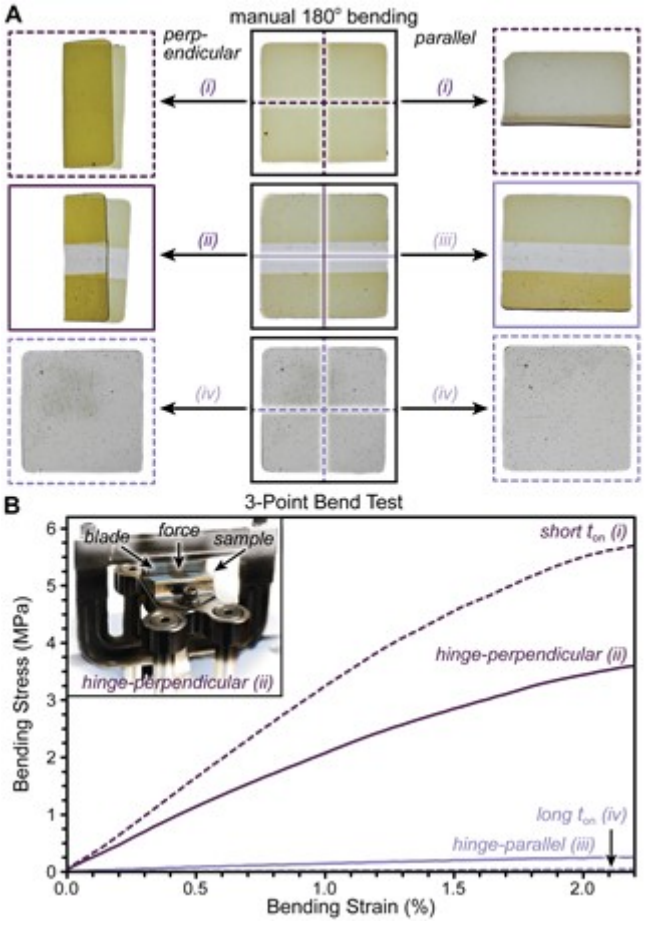

Figure 7. Anisotropic bending with a multimorphic hinge. (A) Backlit images of pure hard (top row), patterned hard-soft-hard (hinge, middle row), and pure soft (bottom row) square samples before (left column) and after perpendicular (middle column) and parallel (right column) 180° bending by hand. (B) Bending stress-strain plot

acquired from a three-point-bend test using DMA. Pure hard and soft samples showed no directional difference.

3. Conclusion

In summary, a photopatternable polyurethane-polyacrylate IPN platform with tunable morphology and mechanical properties was developed by leveraging orthogonal initiation and polymerization mechanisms. Small changes to relative initiation time from a single resin was used to vary IPN morphology and in-turn mechanical properties, with stiffness being tunable by over two orders of magnitude. Short initiation time delay (t_{on}<5 minutes) resulted in large phase separation (up to ~250 nm domains) and opaque bulk materials that behaved as stiff plastics. In contrast, long initiation time delay (t_{on}>5 minutes) resulted in small phase separation (down to <10 nm domains) and transparent bulk materials that behaved as soft elastomers. Photopatterning was employed to produce multimorphic materials, with distinct stiff and soft regions in a single film. This enabled the preparation of materials with uniform composition, yet mechanical anisotropy, as demonstrated by the fabrication and characterization of a hinge. This work is anticipated to inform advanced manufacturing strategies towards multimaterial objects with a diverse array of applications, such as in the area of soft robotics.

Supporting Information

Supporting Information is available from the Wiley Online Library or from the author.

Acknowledgements

This work was primarily supported by the National Science Foundation under Grant No. DMR-2045336 (M.J.A., C. B., and Z.A.P., synthesis and mechanical characterization). Partial support was provided from the U.S. Department of Energy, Office of Science, Basic Energy Sciences under Award #DE-SC0022050 (N.P. and X. G., morphology characterization related to scattering and AFM-IR) and through the Center for Materials for Water and Energy Systems (M-WET), an Energy Frontier Research Center under Award #DE-SC0019272 (M.J.A. and B.D.F., nanoindentation characterization), the National Science Foundation under Grant No. CMMI-2038512 (L.M.C., AFM fast force distance mapping characterization), NSF Graduate Research Fellowship under Grant No. DGE-1610403

(M.J.A.), and the Robert A. Welch Foundation under Grant No. F-2007 (Z.A.P., partial materials and supplies support). The authors acknowledge the use of shared research facilities supported in part by the Texas Materials Institute and the Center for Dynamics and Control of Materials (NSF MRSEC) under Grant No. DMR-1720595.

Received: ((will be filled in by the editorial staff))
Revised: ((will be filled in by the editorial staff))
Published online: ((will be filled in by the editorial staff))

References

[1] N. S. Ha, G. Lu, *Compos. Part B Eng.* **2020**, *181,*

[2] B. S. Lazarus, A. Velasco-Hogan, T. Gómez-del Río, M. A. Meyers, I. Jasiuk, *J. Mater. Res. Technol.* **2020**, *9*, 15705.

[3] N. D. Dolinski, Z. A. Page, E. B. Callaway, F. Eisenreich, R. V. Garcia, R. Chavez, D. P. Bothman, S. Hecht, F. W. Zok, C. J. Hawker, *Adv. Mater.* **2018**, *30*, 1.

[4] V. A. Bobrin, Y. Yao, X. Shi, Y. Xiu, J. Zhang, N. Corrigan, C. Boyer, *Nat. Commun.* **2022**, *13*, 1.

[5] J. J. Schwartz, A. J. Boydston, *Nat. Commun.* **2019**, *10*, 791.

[6] A. K. Rylski, H. L. Cater, K. S. Mason, M. J. Allen, A. J. Arrowood, B. D. Freeman, G. E. Sanoja, Z. A. Page, *Science* **2022**, *378*, 211.

[7] H. Yang, M. Ji, M. Yang, M. Shi, Y. Pan, Y. Zhou, H. J. Qi, Z. Suo, J. Tang, *Matter* **2021**, *4*, 1935.

[8] L. M. Cox, A. K. Blevins, J. A. Drisko, Y. Qi, Y. Ding, C. I. Fiedler-Higgins, R. Long, C. N. Bowman, J. P. Killgore, *Adv. Eng. Mater.* **2019**, 1900578.

[9] B. An, X. Zhao, D. Zhang, *J. Mech. Behav. Biomed. Mater.* **2014**, *34*, 8.

[10] J. P. Gong, Y. Katsuyama, T. Kurokawa, Y. Osada, *Adv. Mater.* **2003**, *15*, 1155.

[11] Q. Chen, H. Chen, L. Zhu, J. Zheng, *Macromol. Chem. Phys.* **2016**, *217*, 1022.

[12] E. Ducrot, Y. Chen, M. Bulters, R. P. Sijbesma, C. Creton, *Science.* **2014**, *344*, 186.

[13] M. S. Silverstein, *Polymer.* **2020**, *207*, 122929.

[14] J.-M. Chenal, D. Colombini, J.-M. Widmaier, *J. Appl. Polym. Sci.* **2006**, *99*, 2989.

[15] M. W. Schulze, L. D. McIntosh, M. A. Hillmyer, T. P. Lodge, *Nano Lett.* **2014**, *14*, 122.

[16] J. M. Widmaier, A. Nilly, J. M. Chenal, A. Mathis, *Polymer.* **2005**, *46*, 3318.

[17] F. Karasu, C. Rocco, M. Lecompère, C. Croutxé-Barghorn, X. Allonas, Y. Zhang, A. C. C. Esteves, L. G. J. van der Ven, R. A. T. M. van Benthem, G. de With, *J. Polym. Sci. Part A Polym. Chem.* **2016**, *54*, 1378.

[18] L. Xu, G. Shan, *Ind. Eng. Chem. Res.* **2013**, *52*, 8216.

[19] J. R. Nowers, B. Narasimhan, *Polymer.* **2006**, *47*, 1108.

[20] O. Konuray, X. Fernández-Francos, X. Ramis, À. Serra, *Polymers.* **2018**, *10*, 178.

[21] D. K. Hohl, A.-C. Ferahian, L. Montero de Espinosa, C. Weder, *ACS Macro Lett.* **2019**, 1484.

[22] R. Raveendran, C. P. Sharma, in *Micro- Nano-Structured Interpenetr. Polym. Networks*, John Wiley & Sons, Inc, Hoboken, NJ, **2016**, pp. 383–397.

[23] *Phase-Separated Interpenetrating Polymer Networks*, Springer Berlin Heidelberg, **2007**.

[24] E. Hasa, J. P. Scholte, J. L. P. Jessop, J. W. Stansbury, C. A. Guymon, *Macromolecules* **2019**, *52*, 2975.

[25] A. J. Silvaroli, T. R. Heyl, Z. Qiang, J. M. Beebe, D. Ahn, S. Mangold, K. R. Shull, M. Wang, *ACS Appl. Mater. Interfaces* **2020**, *12*, 44125.

[26] J. M. Beebe, D. Ahn, D. V Eldred, A. J. Fielitz, T. R. Heyl, M. Lee, S. Mangold, E. Z. Pearce, C. W. Reinhardt, C. Roggenbuck, J. M. Scherzer, K. R. Shull, A. J. Silvaroli, Y. Tan, M. Wang, *Macromolecules* **2022**, *55*, 5826−5839.

[27] E. Pretsch, P. Bühlmann, M. Badertscher, *Structure Determination of Organic Compounds: Tables of Spectral Data*, Springer Berlin / Heidelberg, Berlin, Heidelberg, **2009**.

[28] G. Odian, *Principles of Polymerization*, Wiley-Interscience, Hoboken, NJ, USA, **2004**.

[29] M. Takayanagi, S. Uemura, S. Minami, *J. Polym. Sci. Part C Polym. Symp.* **1964**, *5*, 113.

Multimorphic Materials: Spatially Tailoring Mechanical Properties via Selective Initiation of Interpenetrating Polymer Networks

Table of Contents Graphic

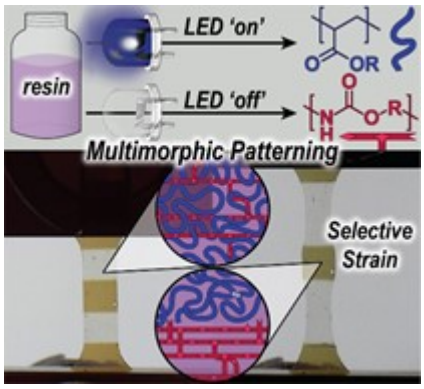

Two disparate polymer networks are created simultaneously using non-interacting chemical reactions and light as a stimulus. Upon turning the light on, the polymers want to phase-separate like oil and water, but the process is hindered as they interlock. Thus, the degree and location of phase separation, and in-turn mechanical properties, can be precisely controlled by the "flick of a switch".